Tuning high-harmonic generation by controlled deposition of ultrathin ionic layers on metal surfaces

Néstor F. Aguirre[1] and Fernando Martín[1,2,3,*]

[1]*Departamento de Química, Módulo 13, Universidad Autónoma de Madrid, 28049 Madrid, Spain*
[2]*Instituto Madrileño de Estudios Avanzados en Nanociencias (IMDEA-Nanociencia), 28049 Madrid, Spain*
[3]*Condensed Matter Physics Center (IFIMAC), Universidad Autónoma de Madrid, 28049 Madrid, Spain*

(Received 4 April 2016; revised manuscript received 25 November 2016; published 19 December 2016)

High-harmonic generation (HHG) from semiconductors and insulators has become a very active area of research due to its great potential for developing compact HHG devices. Here we show, that by growing monolayers (ML) of insulators on single-crystal metal surfaces, one can tune the harmonic spectrum by just varying the thickness of the ultrathin layer, rather than the laser properties. This is shown from numerical solutions of the time-dependent Schrödinger equation for Cu(111)/n-ML NaCl systems ($n = 1-50$) based on realistic potentials. Remarkably, the harmonic cutoff increases linearly with n and as much as an order of magnitude when going from $n = 1$ to 30, while keeping the laser intensity low and the wavelength in the near-infrared range. The origin of this behavior is twofold: the initial localization of electrons in a Cu-surface state and the reduction of electronic "friction" when moving from the essentially discrete energy spectrum associated with a few-ML system to the continuous spectrum (bands) inherent in extended periodic systems. Our findings are valid for both few- and multicycle IR pulses and wavelengths $\sim$1–2 μm.

DOI: 10.1103/PhysRevB.94.245423

I. INTRODUCTION

Discovered in the 1980s [1–3], high-harmonic generation (HHG) has become the fundamental tool of modern attoscience [4–6]. In HHG from atomic or molecular gases, a strong laser field ionizes an electron, which then gains energy from the field and returns to the parent ion, where it finally recombines converting the gained energy into high-frequency radiation [7–10]. The process repeats every half-cycle of the ionizing field, thus leading to a sequence of attosecond light bursts that contain multiples of the fundamental laser frequency, ω_0. Since electronic motion in atomic and molecular systems occurs in the attosecond time scale, light pulses arising from HHG are currently used to probe electron dynamics in those systems [11–18]. Furthermore the HHG process itself contains the signature of the parent-ion dynamics occurring during the round trip of the traveling electron. Thus the analysis of the HHG spectral features can also reveal important aspects of such dynamics [19–25].

HHG from condensed-matter systems was first observed in the mid 1990s [26,27]. In these early experiments, bulk metals and dielectrics irradiated with very intense near-infrared laser fields (of the order of 10^{18} W/cm^2) were shown to emit harmonic radiation as a result of plasma oscillations induced in the system (see also Ref. [28]). Due to the high intensity of the field, HHG was always accompanied by sample damage. More recent experiments have made use of nanotips and nanospheres [29–33], from which HHG has been produced by using relatively moderate fields (of the order of 10^{12} W/cm^2). HHG has also been observed in bulk semiconductors and insulators [34–40] by using similar low intensities (even lower than those usually needed to generate high harmonics in the gas phase) and longer wavelengths, down to the mid infrared (MIR). Under these conditions, no significant damage of the sample is produced. One of the main conclusions of these experiments was that, at variance with HHG in the gas phase, the harmonic cutoff scales linearly with the applied field [34,41,42], which is the consequence of the electron moving in dispersive bands, usually the conduction bands (intraband dynamics [42–44]), and the electron tunneling through the various band gaps accessible in the system (interband dynamics [42,45–49]). Despite its apparent complexity, HHG in bulk semiconductors and insulators has become a very promising area of research, since, e.g., (i) it allows one to reconstruct the band structure of the system [38–40] when more standard condensed-matter techniques do not work, (ii) it is fairly robust against the presence of external fields [39], which is crucial for applications in electronics, (iii) it often leads to multiplateau harmonic spectra [50], and, more importantly, (iv) it opens the way to the fabrication of compact HHG devices.

In this context, it is worth exploring the possibility to modify and eventually control the high-harmonic process by changing the properties of the material, rather than the laser characteristics. An appealing approach is to grow ultrathin layers of insulators (like NaCl, KCl, etc.) on single-crystal metal surfaces. By just varying the thickness of the ultrathin layer, which is a standard procedure in surface physics, one would like to exert some control on the metal response, similar to that required to gradually modify the catalytic activity of metallic species [51–56], to decouple molecules and self-assembled molecular networks from the metal substrate that holds them [57–60], and, what is more important in the context of the present work, to gradually modify the response of metal surface electrons [61–67]. Inspired by the latter works, we propose a similar strategy to tune the harmonic cutoff. To ensure its feasibility, we choose a Cu(111) metallic substrate, which has been widely used to grow NaCl monolayers (ML) leading to Cu(111)/n-ML NaCl composite systems [61–63,68–70]. The Cu(111) surface has an additional advantage: it possesses a localized surface state that lies within the surface-projected band gap [71]. If one considers irradiating the Cu(111) surface with linearly polarized light

*Corresponding author: fernando.martin@uam.es

at grazing incidence, so that polarization goes along the (111) direction, a substantial number of surface electrons will efficiently escape from the metal surface and will be driven into the ultrathin NaCl layer every time the field points outwards the surface (i.e., once every laser cycle), thus avoiding screening and decoherence effects due to metal electrons (NaCl is nearly transparent to IR light and has a refraction index close to 1 [72]). The idea is that Cu electrons initially localized on the surface state will move more efficiently in the NaCl periodic potential than genuine NaCl electrons, since the latter can be more easily ionized.

Here we show, by using realistic potentials for the Cu(111)/n-ML NaCl systems, that the harmonic cutoff increases linearly with the number of NaCl monolayers and as much as an order of magnitude when going from $n = 0$ to 30. This is achieved by using rather low laser intensities, which is a necessary condition to avoid damaging the substrate, and wavelengths of the order of 1–2 μm, i.e., not necessarily in the MIR region. The mechanisms of HHG emission from Cu(111) and ∞ML NaCl/Cu(111) are similar to those already established for gases and bulk semiconductors, respectively. However, the increase and strong variation of the HHG yield with the number of NaCl monolayers is due to a different mechanism: the initial localization of electrons in a Cu-surface state and the decrease of electronic "friction" when moving from a discrete few-ML system to essentially an extended periodic one.

The paper is organized as follows. In Sec. II, we describe the theoretical model that we have used to evaluate the HHG spectra, paying particular attention to the potential energy that describes the interaction of the active electron with the external field and the Cu(111)/n-ML NaCl system. In Sec. III, we present our results, discuss the mechanisms leading to the emission of high-harmonic radiation, and analyze how it is affected by varying the number of NaCl monolayers, the intensity of the applied laser field, and the pulse duration. Finally, in Sec. IV, we summarize the most important conclusions.

II. THEORETICAL MODEL

A. The time-dependent Schrödinger equation

As in previous works [41,42,48], we make use of the single-active electron approximation. The evolution of the electronic quantum state $\psi(z,t)$ is governed by the time-dependent Schrödinger equation (TDSE),

$$i\frac{\partial}{\partial t}\psi(z,t) = H(z,p,t)\psi(z,t) \tag{1}$$

(atomic units are used throughout unless otherwise stated). Here, p is the electron momentum, z is the electron position referred to the Cu(111) image plane, and $H(z,p)$ represents the system's Hamiltonian operator, which is given by

$$H(z,p,t) = H_0(z,p) + \mathcal{V}_l(z,t) - iW(z), \tag{2}$$

where $H_0(z,p)$ is the system's field-free Hamiltonian, $\mathcal{V}_l(z,t)$ is the potential representing the interaction of the active electron with the laser field, and $iW(z)$ is a complex absorbing potential that avoids unphysical reflections of the electronic wave packet on the boundaries of the box used to perform the calculation.

The field-free Hamiltonian is given by

$$H_0(z,p) = \tfrac{1}{2}p^2 + V_i(z), \quad i = \text{ss,val}, \tag{3}$$

where $V_i(z)$ is the effective potential that binds the active electron to the Cu(111)/n-ML NaCl system. We have used two different potentials, labeled as surface-state (ss) and valence-state (val) potentials, to describe HHG from, respectively, the initially localized Cu(111) surface state and a valence state of the n-ML NaCl system. Details about these potentials are given in Sec. II C.

The electron-laser interaction potential is given by (in length gauge)

$$\mathcal{V}_l(z,t) = zS(z,\zeta)F(t)E_0\cos(\omega_0 t), \tag{4}$$

where E_0 is the electric field amplitude, ω_0 the laser frequency (typically in the range 0.8–3.5 μm), and $F(t)$ the pulse envelop. In most examples discussed here, the pulse envelop $F(t)$ is defined as a two-cycle ramp-on $\sin^2$ function followed by a six-cycle flat-top segment and a two-cycle ramp-off $\sin^2$ function (total number of cycles, $T_p = 10$). $S(z,\zeta)$ is a function that accounts for screening of the electric field inside the Cu(111) surface (see, e.g., Ref. [73]). Indeed, the Cu surface is opaque to the IR radiation, so that the laser electric field effectively vanishes after a few atomic layers. This is well represented by the screening function given by

$$S(z,\zeta) = \tfrac{1}{2}\{1 + \tanh[6(z + \zeta/2)/\zeta]\}, \tag{5}$$

where ζ is the screening length. In this work we have chosen $\zeta = 4.0$ a.u. (one atomic layer), but we have checked that results remain unchanged by using $\zeta = 8$ a.u. (two atomic layers) and $\zeta = 12$ a.u. (three atomic layers). We do not need a similar screening factor in the n-ML NaCl region because NaCl is nearly transparent to the IR radiation, although due to surface reflection the effective value of the electric field could be slightly reduced. This effect has not been taken into account in the present work because it only leads to a very small reduction of the HHG emission.

The TDSE has been solved by using a modified version of the split-operator technique [74]. We have used a spatial grid of equidistant points with $\Delta z = 0.1$ a.u. in the interval $z \in [-1500, 1500]$ a.u., a constant time step of 0.01 a.u., and the complex absorbing potential $V_M(z)$ proposed by Manolopoulos [75] located on both sides of the simulation box, namely, $z_l = -1100.0$ and $z_r = 1100.0$ a.u., so that

$$-iW(z) = -iW_M(z - z_l) - iW_M(z - z_r). \tag{6}$$

The harmonic yield has been obtained as the norm square of the Fourier transform of the time-dependent dipole $d_a(t)$, calculated by using the acceleration form of the dipole operator [76],

$$d_a(t) = \langle\psi(z,t)| -\frac{\partial}{\partial z}H(z,p,t)\,|\psi(z,t)\rangle. \tag{7}$$

We have checked the convergence of the calculated dipole by varying both temporal and spatial step sizes, as well as the total simulation time. We have obtained similar harmonic spectra by using the velocity form of the dipole operator, but at the expense of increasing the total simulation time by more than a factor of 5.

B. The choice of the laser parameters

We estimate here the damage thresholds of the Cu(111)/n-ML NaCl system in order to choose a set of laser parameters that is appropriate to observe HHG without destroying the sample. In general, thermal effects like melting and resolidification are less frequently observed with femtosecond laser pulses (as those used here) than with longer pulses. For the former pulses, most morphological damages are due to plasma formation and ablation. The laser fluence threshold for this kind of damage can be estimated by using the model proposed by Gamaly *et al.* [77], which has been checked against experimental results obtained for different materials under different irradiation conditions. In that work, a threshold value of 0.51 J/cm^2 was estimated for copper and we obtain 0.93 J/cm^2 for NaCl (for the latter, we have used the density of free electrons $n_e = 2.23 \times 10^{22}$ cm^{-3}, binding energy of ions in the lattice $\epsilon_b = 7.9$ eV, first ionization potential $J_i = 10.45$ eV, electron mean free path $l_s = 1.9 \times 10^{-5}$ cm, and absorption coefficient $A = 1$). The calculated threshold values are close to the experimental ones reported for copper, 0.5–0.6 J/cm^2 ($\lambda = 780$ nm, pulse duration 150 fs) [78], and NaCl, 1.3 J/cm^2 ($\lambda = 400$ nm, pulse duration 70 fs) [79]. A typical laser frequency used in the present work is $\omega_0 = 0.035\,88$ a.u. (i.e., wavelength $\lambda = 1.27$ μm, optical period $T = 2\pi/\omega_0 \approx 4.2$ fs, and pulse duration $T_p = 10$ cycles) with a maximum peak intensity of 30 TW/cm^2 ($E_0 = 0.030$ a.u.), corresponding to a fluence of 0.32 J/cm^2. This value is significantly lower than the damage threshold for both NaCl and copper. Therefore, we expect that the laser parameters considered in our work will barely lead to any damage of the combined Cu(111)/n-ML NaCl system.

C. Model potential

We have considered two different sources of harmonic generation in this system. Under the action of the strong laser field, electrons can be extracted either from the topmost layers of Cu(111) and then injected into the NaCl bands (initial Cu-surface state) or from the valence band of NaCl and then promoted to the NaCl conduction band (initial NaCl valence state). Here we describe the potential energy terms $V_i(z)$ that describe the interaction of the electron with the Cu(111)/n-ML NaCl lattice in both scenarios.

1. *Model potential for an initial Cu-surface electron*

To represent the interaction of a Cu-surface electron with the Cu(111)/n-ML NaCl lattice, we have used the lateral average of the accurate three-dimensional potential reported by Diaz-Tendero *et al.* [63]. Briefly, the latter potential is defined as

$$V(x,y,z) = V_{\mathrm{Cu(111)}}(z) + V_{\mathrm{NaCl}}(x,y,z) - \Delta W, \qquad (8)$$

where $V_{\mathrm{Cu(111)}}(z)$ is the Cu(111) model potential of Chulkov *et al.* [71] that represents the interaction of the electron with the clean copper surface, $V_{\mathrm{NaCl}}(x,y,z)$ is the change in the interaction due to the presence of the NaCl layers, and ΔW is the change in the work function induced by the NaCl coating (fixed to 1 eV). The $V_{\mathrm{NaCl}}(x,y,z)$ potential accounts for the well-known vertical displacement between the Na^+ and Cl^- ions (rippling), which is nearly zero from the third layer on [63]. Electron-ion interactions were represented by pseudopotentials taking into account the contributions from short-range (Pauli repulsion with core electrons) and Coulomb (position of nuclei) interactions, as well as polarization of the electronic cloud of the ions. To properly account for the dielectric properties of NaCl, electric dipoles induced at NaCl ionic sites were calculated self-consistently, because the dipole induced at one ionic site contributes to the global electric field and thus to the dipoles at other sites [63].

TABLE I. Fitted parameters for the one-dimensional analytical potential shown in Fig. 1. All parameters are given in atomic units.

$a_0 = 0.4453$	$b_0 = 0.0417$	$c_1 = 3.9000$
$a_1 = 0.0136$	$b_1 = 5.0138$	$c_2 = 9.3931$
$a_2 = 0.9369$		$c_i = c_{i-1} + 5.4737$
$a_3 = 13.0123$		$c_n = c_{n-1} + 5.4332$

We have fitted the lateral average of this three-dimensional potential to the formula

$$V_{\mathrm{ss}}(z) = V_{\mathrm{Cu(111)}}(z) - \Delta W + \sum_{i=1}^{n} V_{\mathrm{ion}}(z - c_i) + \sum_{i=1,n} V_{\mathrm{pol}}(z - c_i), \qquad (9)$$

where $V_{\mathrm{ion}}(z - c_i)$ is a pseudopotential representing a NaCl atomic layer centered at $z = c_i$, and $V_{\mathrm{pol}}(z - c_i)$ is an additional polarization potential induced by the metal surface and the vacuum on the first and last monolayers. The latter two terms are given by

$$V_{\mathrm{ion}}(z) = a_0\left[e^{-(z/a_2)^2} - a_1 e^{-(z/a_3)^2}\right],$$
$$V_{\mathrm{pol}}(z) = -b_0 e^{-(z/b_1)^2}. \qquad (10)$$

The values of the coefficients resulting from the fit are given in Table I. For the case of 4 NaCl MLs, Fig. 1 shows that the numerical values (highlighted with red circles) are in excellent agreement with those resulting from the fit (drawn with a blue line). This potential has been extrapolated to include an arbitrary number of NaCl monolayers, by replicating the parameters associated with the third monolayer and using a lattice constant $\ell = 5.4737$ a.u. As can be seen, the atomic positions in the NaCl region are associated with potential maxima, reflecting the fact that the interaction of an external (Cu) electron with the NaCl atomic centers is repulsive. The potential inside the metal reflects the periodic arrangement of the successive Cu(111) planes, which are attractive. This potential reproduces fairly well the surface projected band gap of Cu(111), the energy of the corresponding surface state, and the first three image states of the full-dimensional system.

The initial state used in all calculations based on this potential is the Cu(111) surface state shown in the inset of Fig. 1, which was obtained by using the filtering diagonalization method [80]. As can be seen, in contrast with surface states found in semiconductors and insulators, the Cu(111) surface state goes deep into the bulk, which is due to the rather small surface projected band gap of Cu(111). We note that this surface state is below the Fermi level ($E_f = -0.180$ a.u.), just

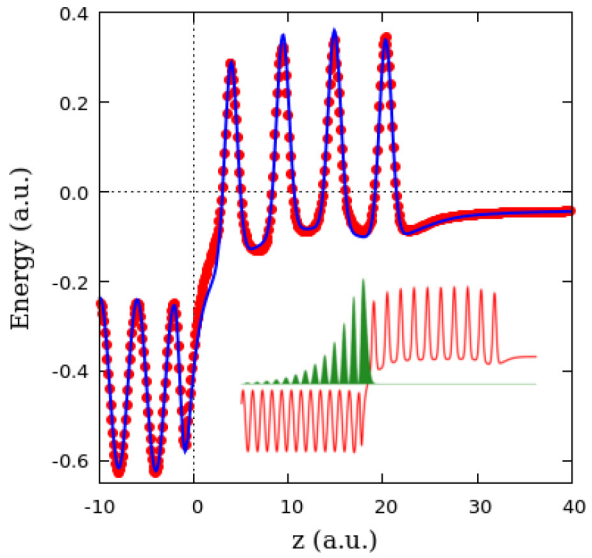

FIG. 1. One-dimensional potential energy model used to describe the interaction of a surface-state electron with the 4NaCl/Cu(111) system. Inset: Sketch of initial state density (surface state) associated with the 10-ML system.

above the Cu valence band, and therefore it is occupied [see Fig. 5(a)]. We have found that the presence of the NaCl layers has a negligible effect on this state, in agreement with previous experimental findings [81].

2. *Model potential for an initial NaCl valence electron*

To obtain the effective potential that a valence-band NaCl electron feels, we have carried out first-principles density functional theory (DFT) calculations and then performed the lateral average of the resulting one-electron Kohn-Sham potential. In more detail, the DFT calculations have been performed with the VASP code (version 5.3.3) [82], by using the Perdew-Burke-Ernzerhof (PBE) [83] generalized gradient approximation (GGA) functional to describe the exchange-correlation energy. The projector augmented-wave (PAW) method [84] has been used to describe the ionic cores. The actual electrons considered in these calculations are Cu($d^{10}p^1$), Na(s^1p^0), and Cl(s^2p^5). Na(s^1p^4) was also used but the resulting potential was identical. A $4 \times 2 \times 1$ Monkhorst-Pack k-point mesh [85] was used for integration over the Brillouin zone (BZ) in combination with a cutoff energy of 300 eV. Due to the incommensurability of the structures between NaCl and Cu(111), we have used a rather large 4×2 supercell containing 2 ML of NaCl and 3 ML of Cu(111), and a vacuum of 15 Å to avoid interslab interactions [see Fig. 2(a)]. We have used the same vertical atomic positions as in the calculations of the potential felt by a Cu-surface electron (see Sec. II C 1).

The resulting laterally averaged potential is shown in Fig. 2(b). This potential has been extrapolated to include an arbitrary number of Cu and NaCl monolayers, by switching on the potential proposed by Chulkov *et al.* [71] beyond the third Cu(111) ML and the potential of bulk NaCl beyond the second NaCl ML, respectively. We have checked that, for an infinite number of NaCl layers, this potential leads to a reasonable

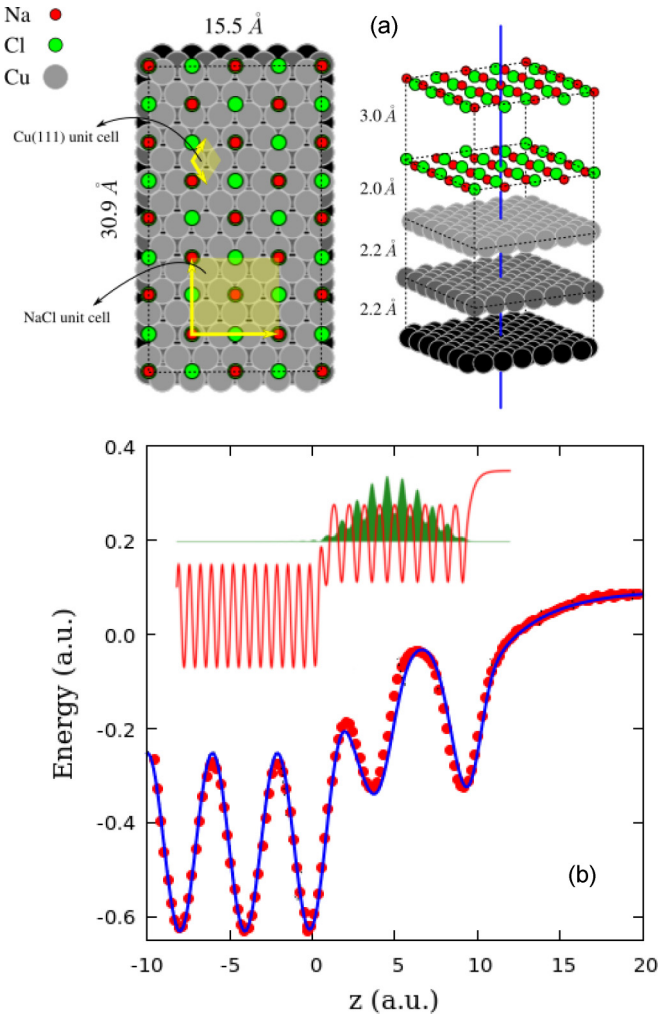

FIG. 2. (a) Supercell geometry used in the calculation of the interacting potential for a valence band electron with the 2NaCl/Cu(111) system. (b) Corresponding laterally averaged potential used in the simulations. Inset: Sketch of initial state density (valence state) associated with the 10-ML system.

description of the band structure of bulk NaCl. We have used the following parametric form to fit this one-dimensional laterally averaged potential:

$$V_{\rm val}(z) = f(c_1' - z)[V'_{\rm Cu(111)}(z) - \Delta W] + f(c_n' - z)f(z - c_1')\left[\sum_{i=1}^{n} V_{\rm ion}(z - c_i) - a_{01}\right] + f(z - c_n')[V_{\rm pol}(z - c_n') - b_{01}], \quad (11)$$

where $f(z) = [1 + \tanh(z)]/2$ is a damping function that ensures the continuity of the potential at the interfaces (copper-NaCl and NaCl-vacuum), $V'_{\rm Cu(111)}(z)$ is the Cu bulk potential introduced by Chulkov *et al.* [71], $V_{\rm ion}(z - c_i)$ is the pseudopotential describing a NaCl atomic layer centered at $z = c_i$, and $V_{\rm pol}(z)$ represents the exponential decay of the potential towards the vacuum. These contributions can be

TABLE II. Fitted parameters for the one-dimensional analytical potential shown in Fig. 2. The values of the parameters not given here are the same as those in Table I. All parameters are given in atomic units.

$a_0 = 0.2975$	$b_0 = 0.3100$	$c_1' = c_1 - 0.3\ell$
$a_1 = 1.4044$	$b_1 = 0.4651$	$c_n' = c_n - 0.1\ell$
$a_{01} = 0.0186$	$b_{01} = 0.0933$	

explicitly written as

$$V_{\mathrm{Cu}}(z) = A_{10} + A_1 \cos\left(\frac{2\pi}{a_s} z\right),$$
$$V_{\mathrm{ion}}(z) = -a_0 e^{-(z/a_1)^2},$$
$$V_{\mathrm{pol}}(z) = -b_0 e^{-b_1 z}. \quad (12)$$

The numerical coefficients resulting from the fit are given in Table II. As can be seen in Fig. 2(b), the results of the fit are in excellent agreement with those resulting from the DFT calculations. At variance with the potential felt by a Cu-surface electron, atomic positions in the NaCl region are associated with potential minima, reflecting the fact that the interaction of a valence electron with the NaCl atomic centers is now attractive. The potential inside the metal remains attractive due to the metallic behavior of copper.

We have employed the Fourier grid Hamiltonian method [86] to evaluate the electronic states associated with this potential. The initial state used in our TDSE calculations for an electron initially bound to the valence shell of NaCl is shown in the inset of Fig. 2(b). This is the lowest state entirely localized on the NaCl subsystem and correlates with the $k = 0$ state of bulk NaCl, where k is the crystal momentum of the electron. As can be seen, this state exhibits maxima over the positions of the NaCl layers [see inset of Fig. 2(b)], which reflects the fact that the electron is mainly localized on the Cl^- ions.

III. RESULTS AND DISCUSSION

A. Cu-surface vs NaCl-valence harmonic emission

Figure 3 shows the calculated harmonic spectra resulting from Cu(111)/n-ML NaCl ($n = 10$, 20, 30, and 40) for electrons departing from the Cu(111) surface state (black lines) and from the NaCl valence-shell state (red lines) described above. The laser wavelength is $\lambda = 1.27$ μm, the duration $T_p = 10$ cycles, and the peak intensity is 20 TW/cm^2. One can see that, when the electron is removed from the valence shell of NaCl, only odd harmonics are emitted in the lower energy region of the spectra (below the 45th harmonic order, approximately). The origin of this effect is similar to that reported for atomic systems: harmonics are generated by electrons moving in a symmetric environment, since, for the lower orders, the motion is confined to the lowest NaCl band, thus reflecting the local symmetry of the potential (the initial electronic state is delocalized over the whole NaCl region). This band is in the middle of the Cu(111) gap and thus electrons moving through it cannot go into the copper surface. However, when electrons are promoted to the second

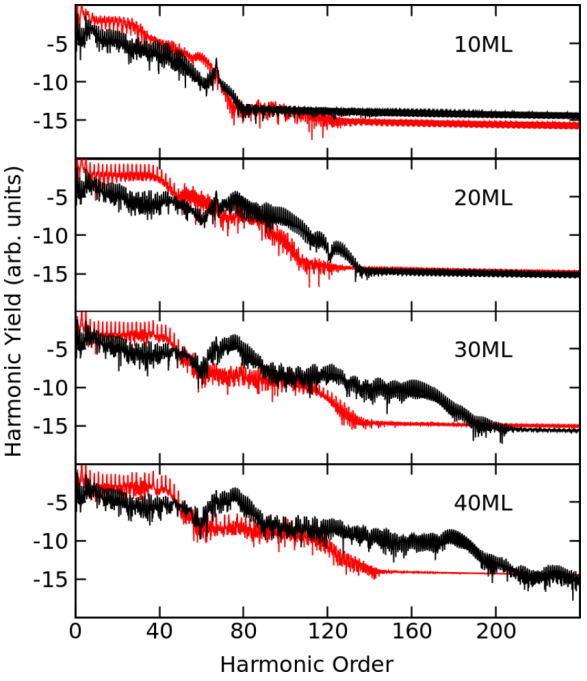

FIG. 3. Comparison of harmonic spectra (in logarithmic scale) for different numbers of MLs of NaCl supported on Cu(111) surface. Red lines represent the harmonic emission for an electron extracted from the valence band of NaCl ($k = 0.0$) and black lines represent the harmonic emission for an electron extracted from the Cu(111) surface state. The laser wavelength is $\lambda = 1.27$ μm, the duration $T_p = 10$ cycles, and the peak intensity is 20 TW/cm^2.

NaCl band (harmonics over the 45th order), they can cross the Cu/NaCl interface and then move through the copper conduction band. Hence, the symmetry is broken and thus both odd and even harmonics are now visible. In contrast, when the electron departs from the Cu-surface state, both odd and even harmonics are observed throughout the whole HHG spectrum, because the initial state is localized on the Cu/NaCl interface and therefore there is never a left-right symmetry.

Figure 3 also shows that, for an electron departing from the NaCl valence shell, the harmonic yield below harmonic 45 increases with the number of NaCl monolayers, while, for an electron departing from the Cu-surface state, it barely changes. This is because, when the initial state is delocalized, as in the first case, each NaCl monolayer becomes a source of active electrons and, consequently, the number of recollision events leading to HHG must increase with the number of monolayers. In contrast, when the initial state is localized, as is the case of the Cu-surface state, there is always a single source of electrons and recollision events leading to HHG are restricted to the interface between Cu(111) and NaCl, which is barely affected by the presence of additional NaCl monolayers.

As can be seen in Fig. 3, contributions from both kinds of electrons are comparable for the lower harmonics, although a bit larger for those originating in the NaCl valence band for the reasons mentioned before. The situation is completely different for the higher harmonics. In both cases, the harmonic cutoff extends to higher orders as the number of NaCl monolayers is increased, but the largest extension is by far the one observed for electrons departing from the Cu-surface state.

For example, in the 40-ML case, the cutoff extension resulting from Cu-surface electrons is twice as large as that resulting from NaCl electrons. And the corresponding harmonic yields differ by almost 8 orders of magnitude in this region.

To get preliminary insight on the mechanisms involved in the HHG process, we have evaluated the intra- and interband dipole transition matrix elements. We have found that the probabilities of interband transitions are on average five times larger in the case of an initial Cu-surface electron than in the case of an initial NaCl-valence electron. This is partly due to the localized nature of the Cu-surface state, which overlaps efficiently with those NaCl states that exhibit a certain degree of localization in the Cu/NaCl boundary. The origin of the latter quasilocalized states is the finite size of the NaCl ML system and has been discussed in earlier work (see, e.g., Refs. [87,88] and references therein). This result explains why the interband mechanism is more efficient in generating harmonics when the electron departs from the Cu-surface state than when it departs from the valence shell of NaCl. Ultimately, as we further elaborate in Sec. III B, this interband mechanism is responsible for (i) the appearance of a sequence of plateaus and (ii) the extension of the harmonic spectra, since the higher the electron progresses in the NaCl bands the higher its kinetic energy. Not surprisingly, the intraband optical transition probabilities are roughly 2 orders of magnitude larger than the interband ones, which is responsible for the systematic reduction of the harmonic yield as one moves along the series of plateaus associated with the different bands.

In the same way, it is also important to point out that depletion of the initial state is only 0.2%–0.4% when the electron starts from the Cu-surface state, while it is substantially larger, around 10%–30%, when the electron comes from the valence shell of NaCl (the lower and upper values correspond, respectively, to the larger and smaller number of NaCl monolayers). In the first case, the (few) missing electrons end up in the copper band, while in the second one, they mainly go into the vacuum, which can be more easily accessed from the valence shell. As a consequence, HHG emission from the initial Cu-surface state approximately remains constant during the whole pulse duration, while that from the valence NaCl monolayers becomes progressively less efficient as time goes by.

B. Variation of the harmonic yield with the number of NaCl monolayers

We focus now on the region of the higher harmonics and the cutoff, which is the most interesting one in view of potential applications. Since harmonic emission in this region is entirely dominated by electrons departing from the Cu-surface state, from now on our analysis is restricted to this particular case.

Figure 4 shows the calculated harmonic spectrum as a function of the number of NaCl layers, n, for a field amplitude/intensity of 0.024 a.u. (123 MV/cm, 20 TW cm^{-2}). As can be seen, the harmonic cutoff increases monotonically with the number of NaCl monolayers, from $\mathcal{N}_c \sim 10$ for 0 ML to $\mathcal{N}_c \sim 180$ for 35 ML, beyond which no further increase is observed. The cutoff scales almost linearly with n and follows the approximate rule $\mathcal{N}_c = 5n$, except for very low n, where the electron motion is either free, because it occurs in the vacuum ($n = 0$), or is hindered by the NaCl potential barriers

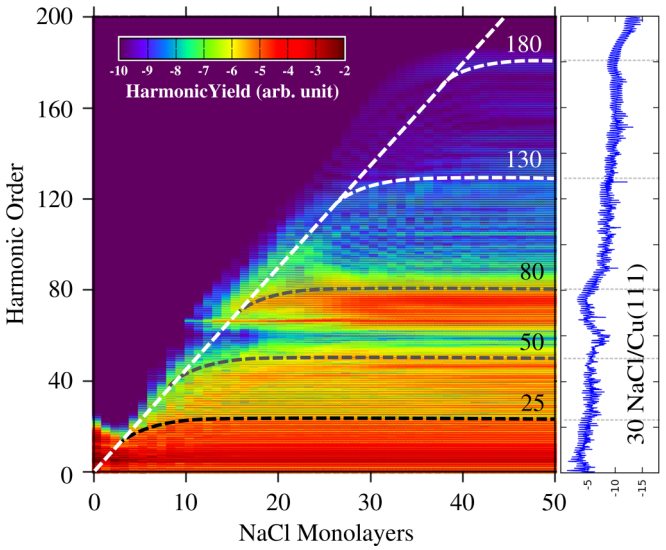

FIG. 4. Left: Harmonic spectra as functions of the number of NaCl monolayers. Right: Harmonic spectrum for the Cu(111)/30-ML NaCl system. Yields are shown in log scale. Laser parameters: $I = 20$ TW/cm^2, $T_p = 10$ cycles, and $\lambda = 1.27$ μm.

($n = 1$ and 2). One can also see the appearance of multiplateau structures, whose number also depends on n. The different plateau limits are indicated by horizontal dashed lines. The first plateau extends up to the 25th harmonic and is only observed for $n \geqslant 5$. This plateau is followed by other ones extending up to the 50th, 80th, 130th, and 180th harmonics for $n \geqslant 10$, 15, 20, and 30, respectively. As can be seen from Fig. 5(c) the plateau appearance thresholds approximately correspond to the top of the NaCl bands, thus suggesting that the NaCl monolayers confine the electron motion to bands and that the transitions between them are at the origin of the observed thresholds: harmonic orders below $\mathcal{N}_c = 25$ would reflect the population of the second band, those between 25 and 50, that of the third band, and so on. This would be similar to the interband mechanism described in previous works (see Refs. [48,89] and references therein). Interestingly, the present results show that the efficiency of such a mechanism increases with the number of overlayers: an increase in n leads to a proportional increase in the intraband density of states (DOS) [see Fig. 5(b)], thus to less "friction" during the intraband motion, and hence to a linear increase of the cutoff with n. The rate of this increase, $\sim$5 harmonic orders per ML, is dictated by the width and height of the potential energy barriers (i.e., by the width of the bands and the gaps) in the n-ML region, thus it can be tuned by using insulators with different lattice constants, e.g., LiF, KCl, etc.

The above mechanism is further confirmed by the windowed Fourier transforms of the time-dependent dipole (Gabor profiles [90]) shown in Fig. 6 for the two extreme cases, clean Cu(111) and Cu(111)/30-ML NaCl, and the 10-ML intermediate case. The chosen time window is described by a Gaussian function of width $1/3\omega_0$. As in the atomic case, high-order harmonics are associated with long Gabor trajectories, which show up when the field reaches its maximum intensity, i.e., after the third cycle of the current pulse. However, the trajectories are seen once every laser cycle instead of once every half cycle, in contrast with atomic systems. This is

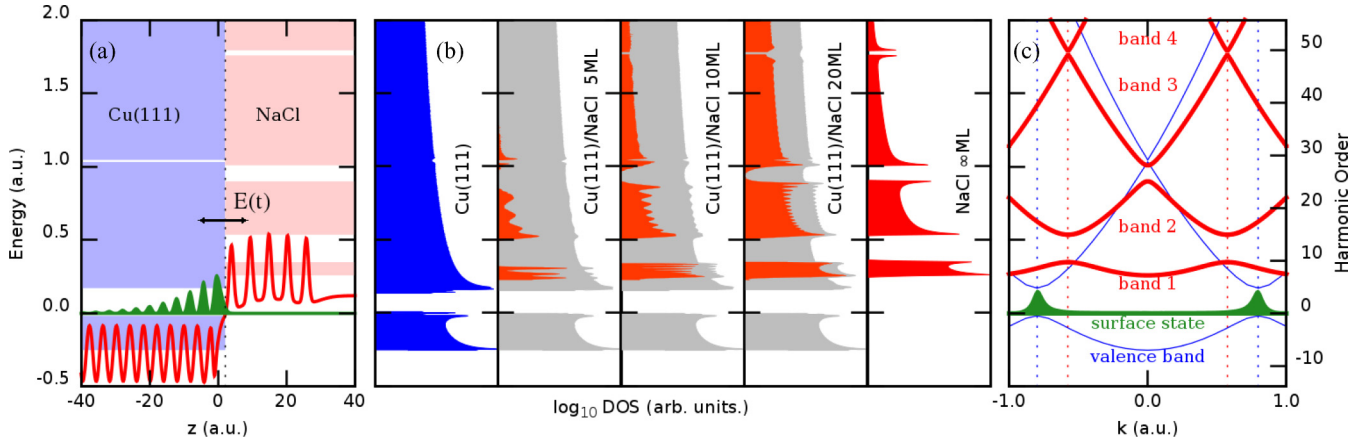

FIG. 5. (a) Potential for the 5-ML NaCl/Cu(111) system (red) and its surface-state density (green). (b) Density of states (DOS) for selected Cu(111)/n-ML NaCl systems (in gray). The red curves represent the relative DOS after removal of the Cu(111) contribution (in blue). (c) Band diagram for Cu(111) (blue) and NaCl (red). Vertical dashed lines indicate the limits of the corresponding first Brillouin zones. The momentum density distribution of the surface state is also shown (green). Due to the localized nature of the surface state, its representation in momentum space corresponds to two well-defined peaks that appear in the limits of the first Brillouin zone of Cu. Harmonic orders are referred to the wavelength $\lambda = 1.27$ μm.

due to screening of the laser field by the Cu electrons, which suppresses all trajectories that start at the Cu(111) surface and then go into the metal (negative field), while trajectories going towards the NaCl layers survive (positive field). For Cu(111) [Fig. 6(a)] the trajectory profiles are very similar to those found in atoms. The situation is completely different in the presence of the NaCl layers [Figs. 6(b)-and 6(c)]. As can be seen, electrons that reach a particular band can either return within the same band or overcome the gap and jump to a higher band, where they go on acquiring kinetic energy before returning. The jumps between bands lead to depletions in the Gabor intensity, since as soon as the electron reaches a new band the electron can more easily progress within this band than go back to the previous one, which requires going through the gap again. In general, interband trajectories follow the applied field and reach their highest energies (cf. harmonic order) at the maximum of that field, while intraband trajectories show up in the Gabor profile as horizontal stripes that depend neither on the field strength nor on the number of NaCl monolayers, but only on the band structure, more specifically on the bands' curvature. It is clear that the most relevant contribution to the cutoff region comes from the interband mechanism, because it allows one to explore larger values of energy, where trajectories are longer and longer and involve more and more bands as n increases.

We have checked that all the above conclusions remain valid for laser wavelengths in the spectral range 1–2 μm (not shown here).

C. Variation of the harmonic yield with laser intensity

Figure 7 shows the variation of the harmonic yield with the field amplitude E_0 for $n = 0$, 10, and 30. For the clean Cu(111) surface, the harmonic cutoff increases with the square of the field, in agreement with the prediction of the three-step model [8], $\mathcal{N}_c = W_s + 3.17E_0^2/4\omega_0^2$ [dashed line in Fig. 7(a)], where $W_s = 0.196$ a.u. is the energy required to excite the surface electron to the Cu conduction band. This is not surprising because the round trip of the electron, initially localized on the surface, occurs in vacuum. The difference in the present case is that such a trip is only possible in half of the accessible space.

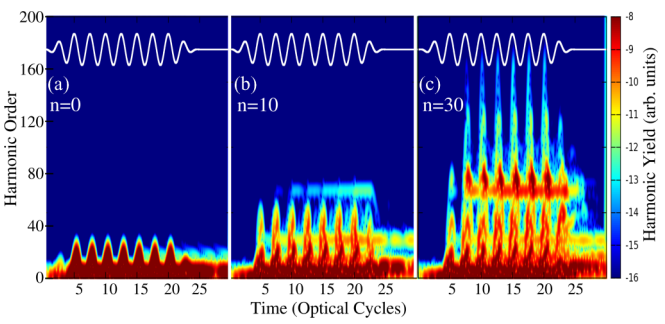

FIG. 6. Time-windowed Fourier transform of the harmonic spectra for Cu(111)/n-ML NaCl. Laser parameters: $I = 20$ TW/cm^2, $T_p = 10$ cycles, and $\lambda = 1.27$ μm.

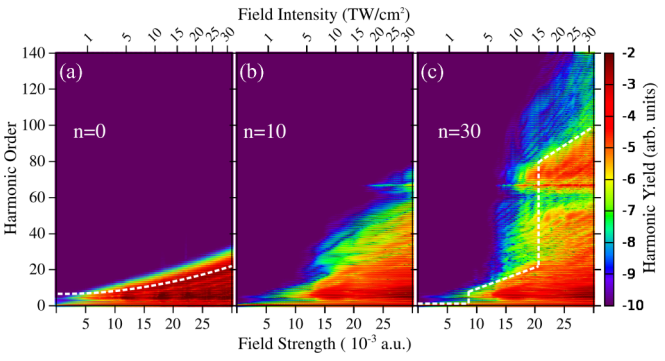

FIG. 7. Harmonic yield as a function of laser field intensity/strength for Cu(111)/n-ML NaCl. Yield is shown in logarithmic scale. See text for details. Laser parameters: $T_p = 10$ cycles and $\lambda = 1.27$ μm. Field strength: 0.0–154.3 MV/cm.

The behavior is much more complex in the presence of NaCl monolayers. For the Cu(111)/30-ML NaCl system [Fig. 7(c)], there are regions where the cutoff increases linearly with E_0 and others where it suddenly increases at specific field values (dashed lines). The first of these sudden increases occurs at $E_0^{(1)} = 0.008$ a.u. This is the value of the field required to first overcome the gap between the Cu(111) surface state and the lowest NaCl, then promote the electron to the top of the latter band, and finally overcome the gap between the first and the second NaCl bands [see Fig. 5(c)]. This effect leads to an extension of the cutoff of about 10 harmonic orders. After this, the cutoff increases almost linearly with E_0 until a second, even more sudden increase occurs at $E_0^{(2)} = 0.021$ a.u.. This is the field needed to additionally promote the electron to the top of the second NaCl band and overcome the gap between this and the third band. As soon as the electron reaches the third NaCl band, there are practically no more gaps to overcome and the electron can easily progress through the band series by means of one-photon resonant transitions near the Brillouin zone, in a way similar to that reported in Refs. [48,89]. This effect leads to an extension of the cutoff by around 100 orders.

As shown by Vampa *et al.* [42], linear scaling with E_0 is the consequence of the electron traveling through energy dispersion bands. The cutoff law resulting from this interband process approximately follows the expression $\mathcal{N}_c^{ij} = [\varepsilon^{ij}(\kappa) - \kappa\, d_k\varepsilon^{ij}(\kappa)] + d_k\varepsilon^{ij}(\kappa)E_0\delta/\omega_0$, where, in our case, i and j refer to two NaCl bands; $\varepsilon^{ij}(k)$ and $d_k\varepsilon^{ij}(k)$ are the corresponding band gaps and k derivatives, respectively; κ is the point in reciprocal space where $\varepsilon^{ij}(k)$ varies almost linearly with k; and $\delta = 1.23$. Figure 7(c) (dashed lines) shows linear cutoff laws derived from this formula for electron-hole pair recollisions coming from bands (2,1) (0.008 a.u. $< E_0 <$ 0.021 a.u.) and (4,1) ($E_0 >$ 0.021 a.u.). For the intermediate 10-ML NaCl/Cu(111) system [Fig. 7(b)], the situation is more subtle. As discussed above, a reduction in the number of NaCl layers leads to a reduction of the DOS within every band and hence to less extended harmonic spectra.

D. Variation of the harmonic yield with pulse duration

We have also performed calculations for a four-cycle pulse ($T_p = 4$, 17 fs) chosen to have the same fluence, 0.32 J/cm^2 (still below the damage threshold), as the ten-cycle pulse used in the previous sections. This corresponds to a maximum field strength of $E_0 = 0.054$ a.u. or an intensity of $I = 10^2$ TW/cm^2. The pulse envelop $F(t)$ has been defined as for the ten-cycle pulse but with no cycles for the flat-top segment. In Fig. 8(a) we compare the harmonic spectra resulting from this pulse with that from the equal-fluence ten-cycle pulse for the Cu(111)/40-ML NaCl system. As can be seen, both spectra show a similar multiplateau structure, but for the shorter pulse the harmonic yield is substantially larger and, remarkably, the cutoff appears at even higher energies. The plateau regions associated with the emission of each band are now more evident, revealing occupations of the seventh ($\mathcal{N}_c < 240$) and eighth NaCl bands ($\mathcal{N}_c < 320$). This is because, although the two pulses have the same fluence, the peak intensity of the few-cycle pulse is substantially larger. The fine structure of these spectra is also different. For the few-cycle pulse, the higher plateaus are regular and the final cutoff is continuous,

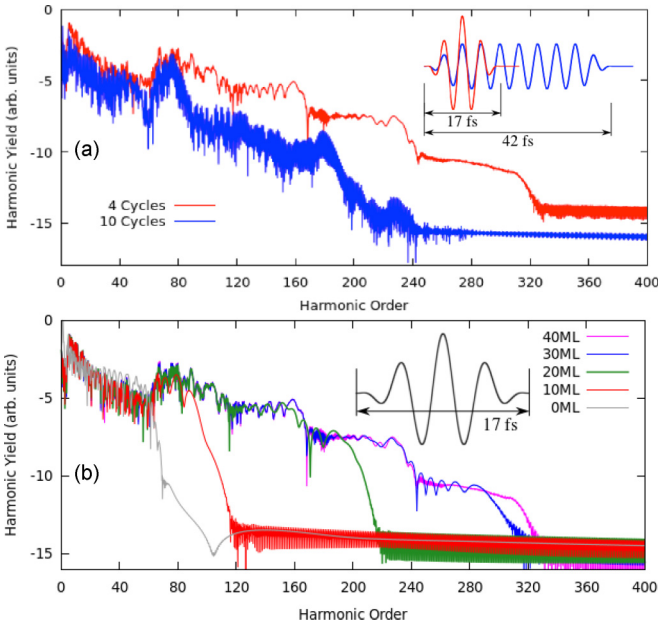

FIG. 8. (a) HH spectrum for the Cu(111)/40-ML NaCl system for the few-cycle (red) and the multicycle (blue) pulses shown in the inset and a common laser fluence of 0.32 J/cm^2. Laser parameter: $\lambda = 1.27$ μm. (b) HH spectra for the Cu(111)/n-ML NaCl systems for the few-cycle pulse shown in the inset and a laser fluence of 0.32 J/cm^2. Laser parameter: $\lambda = 1.27$ μm.

from which a single attosecond pulse of about 150 as could be generated (after high-pass filtering over HH_{270}). In contrast, the plateaus for the multicycle pulse are both irregular and discontinuous, from which a train of attosecond pulses of about 400 as each could be generated (after high-pass filtering over HH_{156}).

Figure 8(b) shows the harmonic spectra for different numbers of NaCl monolayers. As can be seen, the extension of the cutoff with the number of NaCl monolayers is more pronounced for the short pulse than for the long pulse (see Fig. 3). For the four-cycle pulse, the rate of this increase is $\sim$10 harmonic orders per ML, i.e., twice as much as for the ten-cycle pulse, which is a consequence of the electron exploring even higher bands.

IV. CONCLUSION

Our solutions of the TDSE for Cu(111)/n-ML NaCl systems show that harmonic emission plateaus can be extended by more than an order of magnitude by varying the number of NaCl monolayers from 0 to 30. This extraordinarily pronounced cutoff extension is due to harmonic emission from electrons initially localized in the Cu-surface state and scales linearly with the number of NaCl layers as a consequence of the linear increase of the NaCl intraband density of states. The conclusions are valid for both few-cycle and multicycle IR pulses, for wavelengths in the spectral range 1–2 μm, and for peak intensities that lie well below the damage threshold of both Cu and NaCl. This suggests that metal/n-ML insulator systems are ideal candidates to achieve a high degree of control of high-harmonic emission from solids.

ACKNOWLEDGMENTS

We gratefully acknowledge Dr. Sergio Díaz-Tendero for his valuable advice on the construction of the surface potentials. We also acknowledge allocation of computer time at Mare Nostrum Barcelona Supercomputing Center (BSC) and Centro de Computación Científica at Universidad Autónoma de Madrid (CCC-UAM). This work was supported by European Research Council Advanced Grant No. XCHEM 290853, Ministerio de Economía y Competitividad (MINECO) Project No. FIS2013-42002-R, European Cooperation in Science and Technology (COST) Action XLIC CM1204, and the CAM Project NANOFRONTMAG.

[1] A. McPherson, G. Gibson, H. Jara, U. Johann, T. S. Luk, I. A. McIntyre, K. Boyer, and C. K. Rhodes, J. Opt. Soc. Am. B **4**, 595 (1987).
[2] M. Ferray, A. L'Huillier, X. F. Li, L. A. Lompre, G. Mainfray, and C. Manus, J. Phys. B **21**, L31 (1998).
[3] A. L'Huillier and P. Balcou, Phys. Rev. Lett. **70**, 774 (1993).
[4] P. Agostini and L. F. DiMauro, Rep. Prog. Phys. **67**, 1563 (2004).
[5] A. Scrinzi, M. Y. Ivanov, R. Kienberger, and D. M. Villeneuve, J. Phys. B **39**, R1 (2006).
[6] F. Krausz and M. Ivanov, Rev. Mod. Phys. **81**, 163 (2009).
[7] J. L. Krause, K. J. Schafer, and K. C Kulander, Phys. Rev. Lett. **68**, 3535 (1992).
[8] P. B. Corkum, Phys. Rev. Lett. **71**, 1994 (1993).
[9] K. J. Schafer, B. Yang, L. F. DiMauro, and K. C. Kulander, Phys. Rev. Lett. **70**, 1599 (1993).
[10] M. Lewenstein, P. Balcou, M. Y. Ivanov, A. L'Huillier, and P. B. Corkum, Phys. Rev. A **49**, 2117 (1994).
[11] M. Drescher, M. Hentschel, R. Kienberger, M. Uiberacker, V. Yakovlev, A. Scrinzi, T. Westerwalbesloh, U. Kleineberg, U. Heinzmann, and F. Krausz, Nature (London) **419**, 803 (2002).
[12] H. Niikura, F. Légaré, R. Hasbani, M. Y. Ivanov, D. M. Villeneuve, and P. B. Corkum, Nature (London) **421**, 826 (2003).
[13] M. Schultze, M. Ulberacker, T. Uphues, A. J. Verhoef, V. Yakovlev, M. F. Kling, J. Rausehenberger, N. M. Kabachnik, H. Schröder, M. Lezius *et al.*, Nature (London) **446**, 627 (2007).
[14] J. Mauritsson, T. Remetter, M. Swoboda, K. Klünder, A. L'Huillier, K. J. Schafer, O. Ghafur, F. Kelkensberg, W. Siu, P. Johnsson *et al.*, Phys. Rev. Lett. **105**, 053001 (2010).
[15] E. Goulielmakis, Z.-H. Loh, A. Wirth, R. Santra, N. Rohringer, V. S. Yakovlev, S. Zherebtsov, T. Pfeifer, A. M. Azzeer, M. F. Kling *et al.*, Nature (London) **466**, 739 (2010).
[16] H. Wang, M. Chini, S. Chen, C.-H. Zhang, F. He, Y. Cheng, Y. Wu, U. Thumm, and Z. Chang, Phys. Rev. Lett. **105**, 143002 (2010).
[17] C. Ott, A. Kaldun, L. Argenti, P. Raith, K. Meyer, M. Laux, Y. Zhang, A. Blättermann, S. Hagstotz, T. Ding *et al.*, Nature (London) **516**, 374 (2014).
[18] F. Calegari, D. Ayuso, A. Trabattoni, L. Belshaw, S. De Camillis, S. Anumula, F. Frassetto, L. Poletto, A. Palacios, P. Decleva *et al.*, Science **346**, 336 (2014).
[19] M. Lein, Phys. Rev. Lett. **94**, 053004 (2005).
[20] S. Baker, J. S. Robinson, C. A. Haworth, H. Teng, R. A. Smith, C. C. Chirila, M. Lein, J. W. G. Tisch, and J. P. Marangos, Science **312**, 424 (2006).
[21] O. Smirnova, Y. Mairesse, S. Patchkovskii, N. Dudovich, D. Villeneuve, P. Corkum, and M. Y. Ivanov, Nature (London) **460**, 972 (2009).
[22] S. Haessler, J. Caillat, W. Boutu, C. Giovanetti-Teixeira, T. Ruchon, T. Auguste, Z. Diveki, P. Breger, A. Maquet, B. Carré *et al.*, Nat. Phys. **6**, 200 (2010).
[23] A. D. Shiner, B. E. Schmidt, C. Trallero-Herrero, H. J. Wörner, S. Patchkovskii, P. B. Corkum, J.-C. Kieffer, F. Légaré, and D. M. Villeneuve, Nat. Phys. **7**, 464 (2011).
[24] M. Negro, M. Devetta, D. Faccialá, S. De Silvestri, C. Vozzi, and S. Stagira, Faraday Discuss. **171**, 133 (2014).
[25] P. M. Kraus, B. Mignolet, D. Baykusheva, A. Rupenyan, L. Horny, E. F. Penka, G. Grassi, O. I. Tolstikhin, J. Schneider, F. Jensen *et al.*, Science **350**, 790 (2015).
[26] D. von der Linde, T. Engers, G. Jenke, P. Agostini, G. Grillon, E. Nibbering, A. Mysyrowicz, and A. Antonetti, Phys. Rev. A **52**, R25 (1995).
[27] P. Norreys, M. Zepf, S. Moustaizis, A. Fews, J. Zhang, P. Lee, M. Bakarezos, C. Danson, A. Dyson, P. Gibbon *et al.*, Phys. Rev. Lett. **76**, 1832 (1996).
[28] B. Dromey, M. Zepf, A. Gopal, K. Lancaster, M. S. Wei, K. Krushelnick, M. Tatarakis, N. Vakakis, S. Moustaizis, R. Kodama *et al.*, Nat. Phys. **2**, 456 (2006).
[29] S. Kim, J. Jin, Y.-J. Kim, I.-Y. Park, Y. Kim, and S.-W. Kim, Nature (London) **453**, 757 (2008).
[30] M. Schenk, M. Krüger, and P. Hommelhoff, Phys. Rev. Lett. **105**, 257601 (2010).
[31] M. Krüger, M. Schenk, P. Hommelhoff, and M. Kruger, Nature (London) **475**, 78 (2011).
[32] S. Zherebtsov, T. Fennel, J. Plenge, E. Antonsson, I. Znakovskaya, A. Wirth, O. Herrwerth, F. Sussmann, C. Peltz, I. Ahmad *et al.*, Nat. Phys. **4**, 1 (2011).
[33] M. F. Ciappina, J. A. Pérez-Hernández, T. Shaaran, M. Lewenstein, M. Krüger, and P. Hommelhoff, Phys. Rev. A **89**, 013409 (2014).
[34] S. Ghimire, A. D. DiChiara, E. Sistrunk, P. Agostini, L. F. DiMauro, and D. A. Reis, Nat. Phys. **7**, 138 (2011).
[35] B. Zaks, R. B. Liu, and M. S. Sherwin, Nature (London) **483**, 580 (2012).
[36] O. Schubert, M. Hohenleutner, F. Langer, B. Urbanek, C. Lange, U. Huttner, D. Golde, T. Meier, M. Kira, S. W. Koch *et al.*, Nat. Photonics **8**, 119 (2014).
[37] M. Hohenleutner, F. Langer, O. Schubert, M. Knorr, U. Huttner, S. W. Koch, M. Kira, and R. Huber, Nature (London) **523**, 572 (2015).
[38] T. T. Luu, M. Garg, S. Y. Kruchinin, A. Moulet, M. T. Hassan, and E. Goulielmakis, Nature (London) **521**, 498 (2015).
[39] G. Vampa, T. J. Hammond, N. Thire, B. E. Schmidt, F. Legare, C. R. McDonald, T. Brabec, and P. B. Corkum, Nature (London) **522**, 462 (2015).
[40] G. Vampa, T. J. Hammond, N. Thiré, B. E. Schmidt, F. Légaré, C. R. McDonald, T. Brabec, D. D. Klug, and P. B. Corkum, Phys. Rev. Lett. **115**, 193603 (2015).
[41] G. Vampa, C. R. McDonald, G. Orlando, D. D. Klug, P. B. Corkum, and T. Brabec, Phys. Rev. Lett. **113**, 073901 (2014).
[42] G. Vampa, C. R. McDonald, G. Orlando, P. B. Corkum, and T. Brabec, Phys. Rev. B **91**, 064302 (2015).

[43] K. A. Pronin, A. D. Bandrauk, and A. A. Ovchinnikov, Phys. Rev. B **50**, 3473 (1994).
[44] P. G. Hawkins and M. Y. Ivanov, Phys. Rev. A **87**, 063842 (2013).
[45] L. Plaja and L. Roso-Franco, Phys. Rev. B **45**, 8334 (1992).
[46] D. Golde, T. Meier, and S. W. Koch, Phys. Rev. B **77**, 075330 (2008).
[47] P. G. Hawkins, M. Y. Ivanov, and V. S. Yakovlev, Phys. Rev. A **91**, 013405 (2015).
[48] F. Catoire and H. Bachau, Phys. Rev. Lett. **115**, 163602 (2015).
[49] T. Tamaya, A. Ishikawa, T. Ogawa, and K. Tanaka, Phys. Rev. Lett. **116**, 016601 (2016).
[50] C. R. McDonald, G. Vampa, P. B. Corkum, and T. Brabec, Phys. Rev. A **92**, 033845 (2015).
[51] J. Rodriguez, Surf. Sci. Rep. **24**, 223 (1996).
[52] M. Gsell, Science **280**, 717 (1998).
[53] J. Creeley and M. Mavrikakis, Nat. Mater. **3**, 810 (2004).
[54] R. Otero, F. Calleja, V. M. García-Suárez, J. J. Hinarejos, J. de la Figuera, J. Ferrer, A. L. Vázquez de Parga, and R. Miranda, Surf. Sci. **550**, 65 (2004).
[55] G. Laurent, H. F. Busnengo, P. Riviére, and F. Martín, Phys. Rev. B **77**, 193408 (2008).
[56] M. Minniti, D. Farías, P. Perna, and R. Miranda, J. Chem. Phys. **137**, 074706 (2012).
[57] J. Repp, G. Meyer, S. Paavilainen, F. E. Olsson, and M. Persson, Phys. Rev. Lett. **95**, 225503 (2005).
[58] M. Garnica, D. Stradi, S. Barja, F. Calleja, C. Díaz, M. Alcamí, N. Martín, A. L. Vázquez de Parga, F. Martín, and R. Miranda, Nat. Phys. **9**, 368 (2013).
[59] P. Järvinen, S. K. Hämäläinen, K. Banerjee, P. Häkkinen, M. Ijäs, A. Harju, and P. Liljeroth, Nano Lett. **13**, 3199 (2013).
[60] M. Robledo and S. Díaz-Tendero, J. Phys. Chem. C **119**, 15125 (2015).
[61] J. Repp, S. Fölsch, G. Meyer, and K. H. Rieder, Phys. Rev. Lett. **86**, 252 (2001).
[62] L. Gross, F. Mohn, P. Liljeroth, J. Repp, F. J. Giessibl, and G. Meyer, Science **324**, 1428 (2009).
[63] S. Díaz-Tendero, A. G. Borisov, and J.-P. Gauyacq, Phys. Rev. B **83**, 115453 (2011).
[64] M. Barjenbruch, U. Fölsch, and S. Henzel, Surf. Sci. **211-212**, 749 (1989).
[65] M. Kiguchi, G. Yoshikawa, S. Ikeda, and K. Saiki, Phys. Rev. B **71**, 153401 (2005).
[66] G. Kim, J. Kim, W. Jo, D.-H. Son, D.-H. Kim, and J.-K. Kang, Nano Convergence **1**, 27 (2014).
[67] S.-F. Tsay, J. Chung, M.-F. Hsieh, S.-S. Ferng, C.-T. Lou, and D.-S. Lin, Surf. Sci. **603**, 419 (2009).
[68] J. Repp and G. Meyer, Appl. Phys. A **85**, 399 (2006).
[69] S. Fölsch, A. Riemann, J. Repp, G. Meyer, and K. H. Rieder, Phys. Rev. B **66**, 161409 (2002).
[70] R. Bennewitz, J. Phys.: Condens. Matter **18**, R417 (2006).
[71] E. Chulkov, V. Silkin, and P. Echenique, Surf. Sci. **437**, 330 (1999).
[72] H. H. Li, J. Phys. Chem. Ref. Data **9**, 161 (1980).
[73] A. K. Kazansky and P. M. Echenique, Phys. Rev. Lett. **102**, 177401 (2009).
[74] C. Dion, A. Hashemloo, and G. Rahali, Comput. Phys. Commun. **185**, 407 (2014).
[75] D. E. Manolopoulos, J. Chem. Phys. **117**, 9552 (2002).
[76] A. D. Bandrauk, S. Chelkowski, D. J. Diestler, J. Manz, and K.-J. Yuan, Phys. Rev. A **79**, 023403 (2009).
[77] E. G. Gamaly, A. V. Rode, B. Luther-Davies, and V. T. Tikhonchuk, Phys. Plasmas **9**, 949 (2002).
[78] C. Momma, S. Nolte, B. N. Chichkov, F. v. Alvensleben, and A. Tünnermann, Appl. Surf. Sci. **109-110**, 15 (1997).
[79] M. Hada, D. Zhang, K. Pichugin, J. Hirscht, M. A. Kochman, S. A. Hayes, S. Manz, R. Y. Gengler, D. A. Wann, T. Seki *et al.*, Nat. Commun. **5**, 3863 (2014).
[80] Ğ. Barinovs and G. Nyman, Chem. Phys. **281**, 23 (2002).
[81] J. Repp, G. Meyer, and K.-H. Rieder, Phys. Rev. Lett. **92**, 036803 (2004).
[82] G. Kresse and J. Furthmüller, Phys. Rev. B **54**, 11169 (1996).
[83] J. P. Perdew, K. Burke, and M. Ernzerhof, Phys. Rev. Lett. **77**, 3865 (1996).
[84] G. Kresse and D. Joubert, Phys. Rev. B **59**, 1758 (1999).
[85] J. C. Phillips, Phys. Rev. **112**, 685 (1958).
[86] C. C. Marston and G. G. Balint-Kurti, J. Chem. Phys. **91**, 3571 (1989).
[87] S. B. Zhang, C.-Y. Yeh, and A. Zunger, Phys. Rev. B **48**, 11204 (1993).
[88] V. I. Gavrilenko and F. Koch, J. Appl. Phys. **77**, 3288 (1995).
[89] M. Wu, S. Ghimire, D. A. Reis, K. J. Schafer, and M. B. Gaarde, Phys. Rev. A **91**, 043839 (2015).
[90] D. Gabor, J. Inst. Electr. Eng. London **93**, 429 (1946).